Proceedings of the ASME 2015 Pressure Vessels & Piping Conference
PVP 2015
July 19-23, 2015, Boston, Massachusetts, USA

FINAL PVP2015-45242

MEASUREMENTS OF FATIGUE CRACK GROWTH RATES OF THE HEAT-AFFECTED ZONES OF WELDS OF PIPELINE STEELS*

Andrew J. Slifka
NIST, Applied Chemicals and Materials Division
Boulder, Colorado, USA

Elizabeth S. Drexler
NIST, Applied Chemicals and Materials Division
Boulder, Colorado, USA

Robert L. Amaro†
NIST, Applied Chemicals and Materials Division
Boulder, Colorado, USA

Damian S. Lauria
Laboratory Automation, Inc.
880 Sunshine Canyon
Boulder, Colorado USA

Louis E. Hayden
Louis E. Hayden Associates
Bethlehem, Pennsylvania, USA

Christopher N. McCowan‡
NIST, Applied Chemicals and Materials Division
Boulder, Colorado, USA

Jeffrey W. Sowards
NIST, Applied Chemicals and Materials Division
Boulder, Colorado, USA

ABSTRACT

Pipelines are widely accepted to be the most economical method for transporting large volumes of hydrogen, needed to fuel hydrogen-powered vehicles. Some work has been previously conducted on the fatigue crack growth rates of base metals of pipeline materials currently in use for hydrogen transport and on pipeline materials that may be used in the future. However, welds and their heat-affected zones are oftentimes the source and pathway for crack initiation and growth. The heat-affected zones of welds can exhibit low resistance to crack propagation relative to the base metal or the weld itself. Microstructural irregularities such as chemical segregation or grain-size coarsening can lead to this low resistance. Therefore, in order to have adequate information for pipeline design, the microstructures of the heat-affected zones must be characterized, and their mechanical properties must be measured in a hydrogen environment. With that in mind, data on the fatigue crack growth rate is a critical need. We present data on the fatigue crack growth rate of the heat-affected zones for two girth welds and one seam weld from two API 5L X52 pipes. The materials were tested in hydrogen gas pressurized to 5.5 MPa and 34 MPa at a cyclic loading rate of 1 Hz, and an *R* ratio of 0.5.

NOMENCLATURE

CMOD = crack mouth opening displacement
CT = compact tension
FCGR = fatigue crack growth rate
HAZ = heat affected zone (of a weld)
ΔK = stress intensity factor range
W = specimen length

INTRODUCTION

As demand for hydrogen rises with the anticipated influx of hydrogen fuel-cell vehicles, transport of hydrogen fuel will have to shift from trucks to a more economical means. Pipelines are the most economical means of transporting fuel in the US. In order to use pipelines to transport pressurized hydrogen gas, the effects of hydrogen on these ferritic steels needs to be measured. There exists a large body of research on pipeline steels under monotonic tensile loading, much of the work done in hydrogen gas [1-13]. However, it is likely that a pipeline would fail by fatigue, and therefore, fatigue data on pipeline steels is required. Additionally, FCGR data can be used by pipeline designers to aid in the determination of the lifetime of a pipeline. Fatigue measurements in hydrogen have been performed on pipeline steel base metals, and even some on welds [3, 14-23]. Cracks can initiate and grow in or near the seam or girth welds in a pipeline. Only recently has any work been published on fatigue of HAZs in hydrogen [24, 25].This work discusses FCGR results from the HAZs of 3 of the 4 welds (both girth and vintage seam) from a modern and a vintage X52 pipe.

* Contribution of the National Institute of Standards and Technology, an agency of the US government; not subject to copyright in the USA.
† Current affiliation, Associate Professor, Dept. of Mech. Eng. Colorado School of Mines, 1500 Illinois St, Golden, Colorado 80401
‡ Current affiliation, Contractor, Protiro, Inc., 3401 Quebec St., suite 6500, Denver, Colorado 80207

 Copyright © 2015 by ASME

MATERIALS, TEST MATRIX, AND METHODS

Materials

The materials used for this study were from vintage (ca. 1964) X52 and modern (ca. 2011) X52 pipeline steels. The HAZs of both the seam and girth welds of the vintage X52 pipeline were tested, and the HAZ of the girth weld of the modern X52 pipeline was tested. The reasoning for including these two was to test an older steel that could be a candidate for re-purposing a pipeline section for hydrogen use and to test a modern steel that is now in hydrogen service. The HAZ of the seam weld of the modern X52 pipe was not tested at this time, but will be included in a later study.

Table 1 shows the tensile properties of base metal, HAZ, and weld, measured in air in the transverse or radial (perpendicular to the direction of fluid flow in the pipe and the rolling direction) orientation, except for the seam weld for the vintage pipe, which was measured in the longitudinal (axial), or flow, direction. The yield stress is defined as the 0.2 % offset from the linear elastic line. For each condition, base metal, HAZ, or weld, at least 3 specimens were tested. The size of the modern pipe is 508 mm (20 inch) in diameter with a wall thickness of 10.6 mm. The size of the vintage pipe is 914 mm (36 inch) in diameter with a wall thickness of 10.6 mm. Note that the vintage X52 base metal did not reach the specified minimum yield strength (SMYS) of 360 MPa (52 ksi). The reason for this is unknown. The modern X52 material qualifies as an X70, since the yield strength is above 483 MPa (70 ksi). Both welds for the vintage pipe have overmatched yield strengths, compared to respective base metals. The strength of the girth weld from the modern pipe is slightly undermatched to the base metal.

Table 1. Tensile properties of the fusion zones, HAZs, and base metals for the two X52 steels (σ_y from 0.2 % offset). Orientations all transverse except seam weld and seam (S) HAZ.

Material	σ_y [MPa ± std. dev.]	σ_{UTS} [MPa ± std. dev.]
X52 Modern, Girth Weld	463 ± 5	567 ± 5
X52 Vintage, Girth Weld	428 ± 5	520 ± 5
X52 Vintage, Seam Weld	425 ± 5	529 ± 5
X52 Modern, G HAZ	463 ± 5	526 ± 5
X52 Vintage, G HAZ	372 ± 5	531 ± 5
X52 Vintage, S HAZ	462 ± 5	551 ± 5
X52 Modern, Base metal	487 ± 5	588 ± 5
X52 Vintage, Base Metal	325 ± 4	526 ± 4

Table 2 shows the chemistries of the two steels; the corresponding girth-weld chemistries are given in Table 3. Carbon content is low in modern steels to improve weldability. A large difference can be seen between the base metals of the vintage steel and the modern steel, such as, the vintage steel has more than three times the carbon content of its modern counterpart. The modern steel has low sulfur content and contains the micro-alloying elements vanadium, niobium and titanium. Both X52 steels are low in molybdenum. The chemistries of the welds are somewhat similar for the vintage and modern girth welds, in that neither has significant microalloying elements. The modern girth weld has higher manganese, nickel and chromium for strengthening, whereas the vintage girth weld has lower manganese, but high molybdenum for strengthening.

Table 2. Chemistries of the X52 base metals, in mass percent.

Element	C	Mn	P	S	Si	Cu	
X52_vintage	0.238	0.960	0.011	0.021	0.064	0.085	
X52_modern	0.071	1.060	0.012	0.004	0.240	0.016	
Element	**Ni**	**Cr**	**Mo**	**V**	**Nb**	**Ti**	**Al**
X52_vintage	0.050	0.014	0.004	0.002	0.001	0.002	0.002
X52_modern	0.016	0.033	0.003	0.004	0.026	0.038	0.017

Table 3. Chemistries of the X52 girth welds, in mass percent.

Element	C	Mn	P	S	Si	Cu	
X52 Vintage GW	0.110	0.350	0.009	0.025	0.100	0.024	
X52 Modern GW	0.130	0.780	0.010	0.013	0.150	0.026	
Element	**Ni**	**Cr**	**Mo**	**V**	**Nb**	**Ti**	**Al**
X52 Vintage GW	0.046	0.018	0.430	0.006	0.001	0.005	0.010
X52 Modern GW	0.610	0.110	0.093	0.003	<0.001	0.009	0.006

Microstructure

The base metal (Figure 1, left) from the vintage steel is a blend of approximately 70 % polygonal ferrite and 30 % pearlite with an average grain size of approximately 30 μm. The girth weld HAZ closest to the unaffected base metal has ferrite plus degenerate pearlite. Moving closer to the weld fusion zone (Figure 1, center), where the peak temperature was high enough to partially austenitize the pipe material, the grains exhibit some refinement, and the microstructure includes polygonal ferrite, acicular ferrite, and tempered martensite (where tempering occurs due to subsequent weld passes in the multipass welding process). There is a large distribution of grain sizes in this part of the HAZ. The HAZ at the cap and root passes of the weld exhibits large grains of untempered martensite. The microstructure at the root and cap passes is indicative that those passes occurred after the fill passes. The weld zone, shown on the right of Fig. 1, is a mixture of polygonal ferrite, acicular ferrite, and dispersed carbides.

Copyright © 2015 by ASME

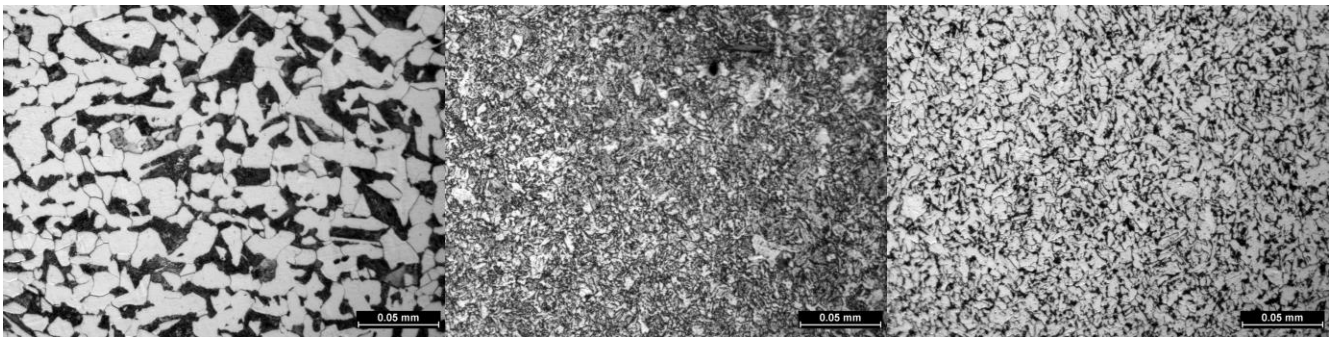

Figure 1. Optical microscope images of, from left to right, base metal, HAZ, and girth weld fusion zone from the X52 vintage material. Longitudinal – circumferential plane.

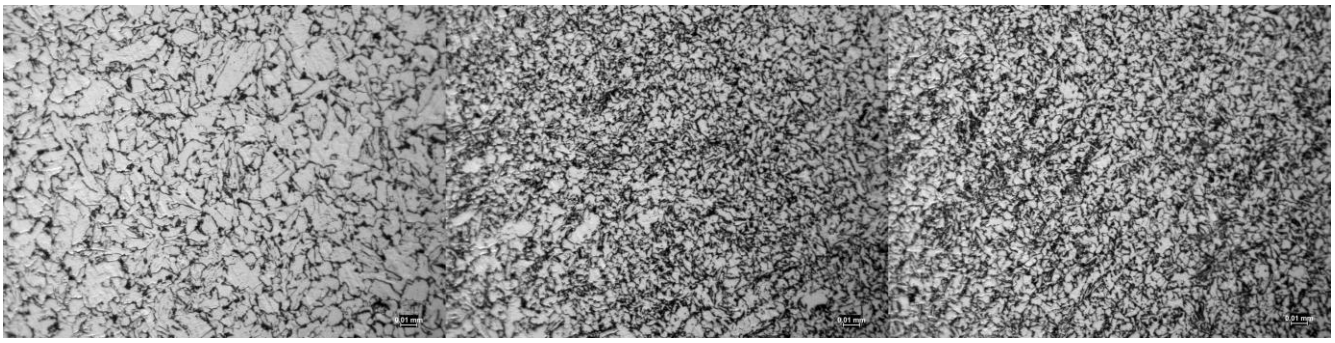

Figure 2. Optical microscope images of, from left to right, the base metal, HAZ, and girth weld fusion zone from the X52 modern material. Longitudinal – circumferential plane.

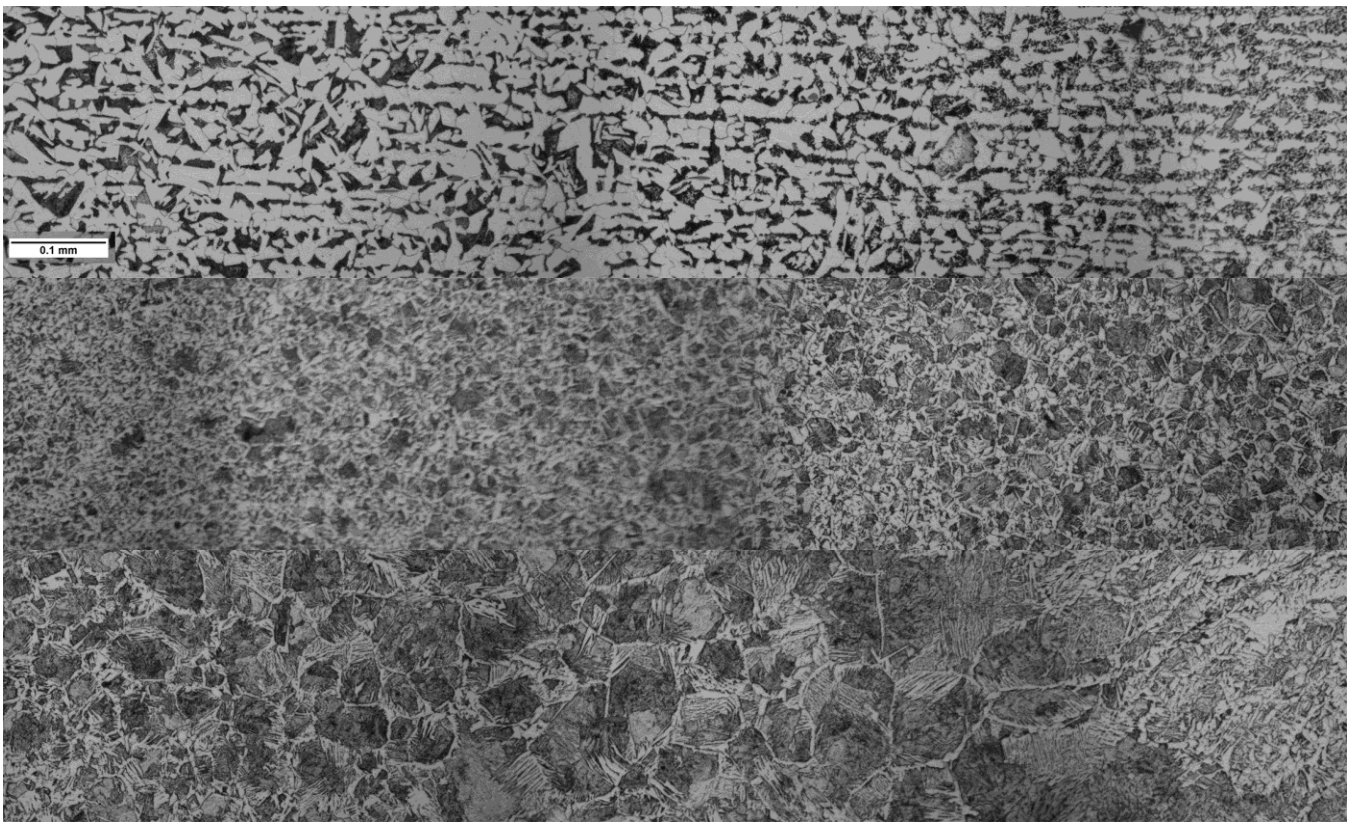

Figure 3. X52 vintage seam weld, with base metal in the upper left, transitioning to HAZ and weld fusion zone from top to bottom and left to right. Longitudinal – circumferential plane.

Copyright © 2015 by ASME

Qualitative estimates of the modern X52 microstructure show that the base metal has over 90 % polygonal ferrite, 5 to 10 % acicular ferrite, and 1 to 2 % well-dispersed carbides. The average grain size is ~10 µm. Figure 2 shows the base metal, HAZ, and girth weld fusion zone, from left to right. The weld fusion zone, shown on the right of Fig. 2, has finer microstructure than the base metal. This girth weld microstructure consists of a mixture of more than half acicular ferrite, polygonal ferrite, and dispersed carbides. The HAZ has a distribution of grain sizes that, as expected, falls between that of the base metal and weld. The HAZ has a mixture of polygonal ferrite, acicular ferrite, and carbides. The heat from the welding process austenitized the grains in the base metal and refined the grains during cooling. The modern steel had no significant microstructural banding, but the base metal of the vintage steel showed large-scale alternating bands of mostly ferrite and mostly pearlite.

The seam weld and associated HAZ of the vintage pipe had a more varied microstructure than that of either of the girth welds. The modern girth weld was a gas metal arc weld (GMAW) and the vintage was a submerged metal arc weld (SMAW). The seam weld was made by way of a shielded metal arc weld (SAW) process. The microstructure is shown in stacked strips in Figure 3, moving from base metal on top and left to weld fusion zone on bottom and right. Compared with the 9-pass weld plus root and cap for the girth weld, this SAW is a two-pass weld that uses a much higher heat input per pass, resulting in a ~3 mm wide HAZ. The outer part of the HAZ, near the unaffected base metal, is ferrite plus degenerate pearlite. The HAZ microstructure changes significantly closer to the weld. Past the region of degenerate pearlite, the temperature was high enough for austenitization, because the grains are refined, with a resulting microstructure of polygonal ferrite plus acicular ferrite, plus martensite. The partial austenitization results in carbon-enriched austenite that cools during weld cooling and transforms into martensite. The austenite grain size increases nearer to the fusion zone during austenitization. This gives way to increasing martensite as the grains coarsen, with grain boundary ferrite on the outer edges. Near the fusion line, the grains are greatly enlarged up to 100 µm in size. The seam weld contains widmanstatten and polygonal ferrite, which formed upon cooling.

Test Methods

All FCGR measurements were done at a load ratio, R, of 0.5 and a loading frequency of 1 Hz. Baseline measurements were done in air at 1 Hz. Test pressures of 5.5 MPa and 34 MPa hydrogen gas were used.

The tensile tests were done in accordance with ASTM E8 [26]. FCGR tests were done in accordance with ASTM E647 for CT specimens with a CMOD gauge attached to the load line and W=45 mm, where W is the specimen width [27]. The thickness of all weld and HAZ specimens ranged between 8 mm and 12 mm. The specimens were polished to an average surface roughness of less than 0.25 µm, in accordance with ASTM G142 [28]. For the CT specimens corresponding to the HAZ of the seam weld, the crack runs parallel to the axial pipe direction, along the weld direction, and the force is exerted in the transverse, or hoop stress, direction, designated as T-L. For the specimens corresponding to the HAZs of the girth welds, the orientation is such that the crack runs along the girth weld direction, and the load is applied in the axial pipe direction, designated L-T. All CT specimens were fatigue pre-cracked in air to obtain a sharp initial crack. Most welds, particularly girth welds, have a V-shape to them, in cross section. Therefore, it is advantageous to tilt the CT specimens to maximize the probability that the fatigue crack starts entirely in the HAZ and stays there for the duration of the test. However, these materials were too thin to allow specimens to be made with an off-plane tilt. Future post-test analysis will show whether the crack deviated from the HAZ or not. Figure 4 shows a drawing of the alignment of the crack with the HAZ for these measurements. Most of the fatigue data from this work used an apparatus that can simultaneously test 10 specimens, and is described elsewhere [29, 30]. Tests were run in a chamber capable of hydrogen gas pressures up to 34 MPa. Ultra-pure (99.9999 %) helium was used for purging the chamber and ultra-pure (99.9995 %) hydrogen was used for testing. Test pressure was maintained to within 3 % of the target pressure throughout the duration of each experiment. Details of the purging procedure can be found elsewhere [30]. Analysis of the test gas showed that the hydrogen had less than 1 ppm water and less than 1 ppm oxygen for these HAZ tests. HAZ specimens tested at 5.5 MPa hydrogen gas pressure were run simultaneously in the same set. All other specimens were not run in the same set.

Test Matrix

One or two specimens from the girth weld and associated HAZ were tested at each pressure for the vintage material. The HAZ from the seam weld of the vintage pipe was tested at 5.5 MPa, and the HAZ associated with the girth weld of the modern pipe was tested at 34 MPa. Future tests are planned to complete the test matrix of two tests for each material at each condition.

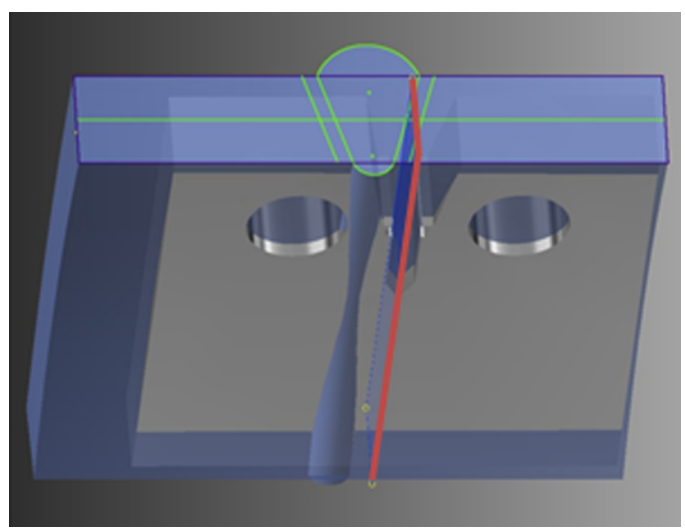

Figure 4. Drawing of a CT specimen showing where the fatigue crack is intended to run (red) relative to the weld and HAZ (green).

Copyright © 2015 by ASME

RESULTS AND DISCUSSION

The base metals of these pipes have previously been measured for FCGR in pressurized hydrogen gas [22, 23]. FCGR measurements of the HAZ of the girth weld of the vintage material are shown in Fig. 5. The base metal, both in hydrogen and in air, is given in the form of thick lines, with air in green, 5.5 MPa hydrogen gas in red, and 34 MPa hydrogen gas in purple. These lines come from visual fits of at least 3 measurements, each. The width of each line shows the spread of the multiple measurements at that test condition, and roughly approximate the uncertainty of the measurement for that condition. The actual calculated uncertainty of the measurement method can be found in [29].

With reference to the vintage pipe, the two measurements of the HAZ of the girth weld at 5.5 MPa hydrogen gas pressure lie mostly within the range of base metal, for the same test condition, and show little variability. The HAZ of the girth weld at 34 MPa hydrogen gas pressure lies within the range of the base metal data, and are significantly higher than the 5.5 MPa case. This test of the HAZ of the girth weld provided data at low values of ΔK, which were not obtained for base metal. The sensitivity of FCGR for the girth weld HAZ to hydrogen gas pressure is similar to that of the base metal.

FCGR measurements were also made on the girth weld of the vintage pipe. Figure 6 shows a comparison of FCGR data between the girth weld (open symbols) and associated HAZ (closed symbols) at two hydrogen gas pressures, 5.5 MPa and 34 MPa. The weld data appear slightly lower in FCGR than that of the HAZ, but are within the uncertainty exhibited by the base metal at that pressure. With just two specimens tested from the vintage material, neither FCGRs of the weld nor HAZ show enough variance from that of the base metal to support the premise that they fall outside of the uncertainty of the measurement, despite the differences in microstructure between base metal, HAZ, and weld. Again, a strong pressure effect is apparent, particularly at ΔK values below ~12 MPa-m$^{1/2}$.

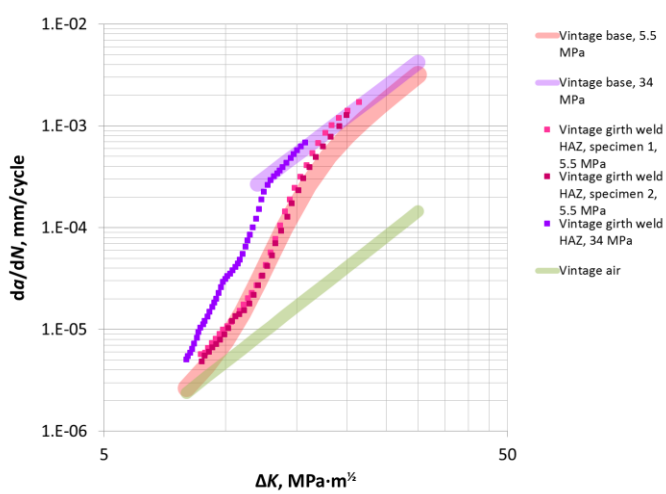

Figure 5. FCGR data on the vintage X52 steel in air, 5.5 MPa hydrogen, and 34 MPa hydrogen, comparing base metal with the HAZ of the girth weld.

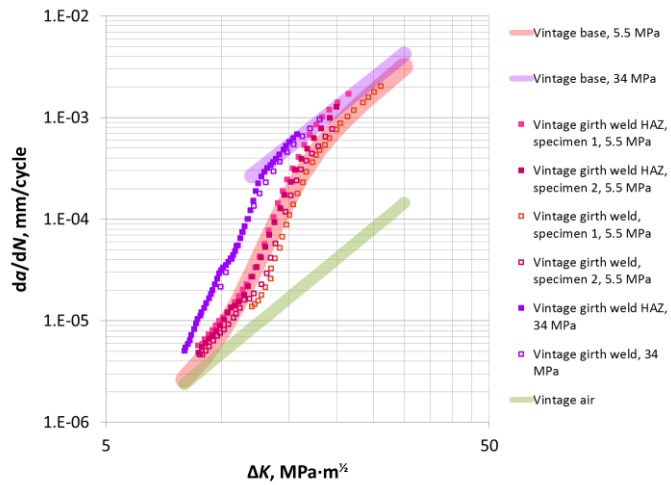

Figure 6. Comparison between FCGR data for the girth weld and HAZ of the vintage X52 steel.

The FCGR of the HAZ of the girth weld, sectioned from the modern steel, was measured at 34 MPa hydrogen gas pressure. Figure 7 shows FCGR data comparing girth weld HAZ to base metal for the modern material. The HAZ data from the girth weld of the vintage pipe is also included for comparison. FCGR data was measured only at 34 MPa for this girth weld. The base metal of the modern X52 has less pressure sensitivity than does the vintage material, and the FCGR data at 34 MPa for the HAZ of the girth weld of the modern material lies just below that of the base metal. At 34 MPa hydrogen gas pressure, the HAZ of the girth weld of the modern pipe has lower FCGR than that of base metal and the corresponding HAZ of the vintage X52 material, but all three lie within the uncertainty of the measurement.

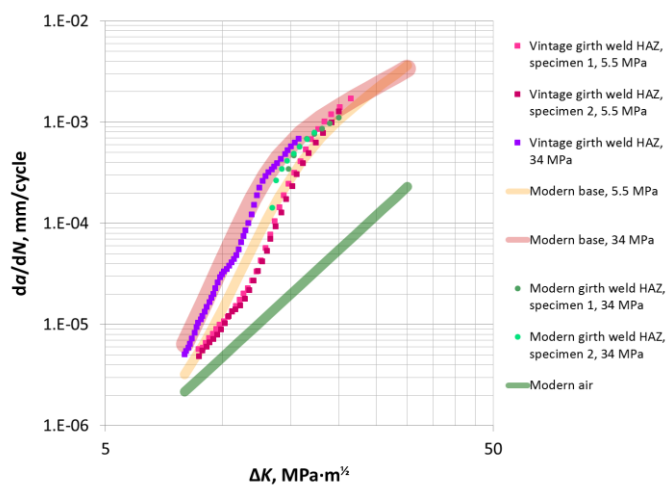

Figure 7. FCGR data for the HAZ of the girth weld of the modern X52 steel. Fits to base metal data in air, 5.5 MPa and 34 MPa hydrogen gas, and HAZ data from the girth weld of the vintage steel are shown for comparison.

Copyright © 2015 by ASME

The two measurements of the HAZ of the seam weld from the vintage pipe, at 5.5 MPa hydrogen gas pressure, show a substantial divergence. The FCGR data is shown in Figure 8. One test is consistent with the FCGR of base metal, and the other yielded data at a higher FCGR than base metal. These specimens were extracted from the weld side-by-side, and tested

simultaneously in the multiple-specimen chamber. Still, the spread of the seam weld data is not surprising. Figure 9 shows a composite image of the entire weld and HAZ shadowing. Because of the slanted geometry of the weld and the small thickness of the pipe, we cannot obtain a vertical "cut" that contains just HAZ for the crack to fatigue through. This issue pertains to all three welds in this work. An additional issue is that when we have specimens machined, the likelihood of having the crack run through the same exact amount of HAZ and weld is low. The approximate placement of the cracks is given by blue and red lines in Fig. 9 for the two seam HAZ specimens tested. The difference in the ratio of HAZ to weld that the crack runs through, based on the placement of the fatigue crack, could possibly yield a variation in the residual stresses, which can greatly affect crack growth. This may be the case for any weld, and therefore for any data for weld or HAZ shown in this work. However, the extraction of these specimens from the pipes might relieve the residual stresses to the point where they do not affect FCGR. Measurement of residual stresses should be performed in order to determine whether the magnitudes could affect FCGR.

The variation of microstructure that the fatigue crack runs through can also contribute to differences in fatigue crack growth from one specimen to another. For instance, the crack path associated with the vintage seam weld HAZ, specimen 2, shown in Fig. 8, likely contains more of the large-grained martensitic regions of microstructure than that of specimen 1. Note the dark structure directly adjacent to the fusion zone in the HAZ in Fig. 9 (shown at a higher magnification in the lower strip of Fig. 3),

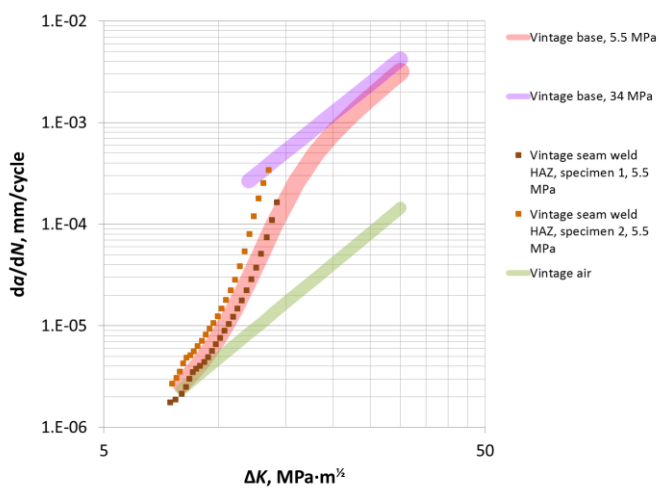

Figure 8. FCGR data on the vintage X52 steel in air, 5.5 MPa hydrogen, and 34 MPa hydrogen, comparing base metal with the HAZ of the seam weld.

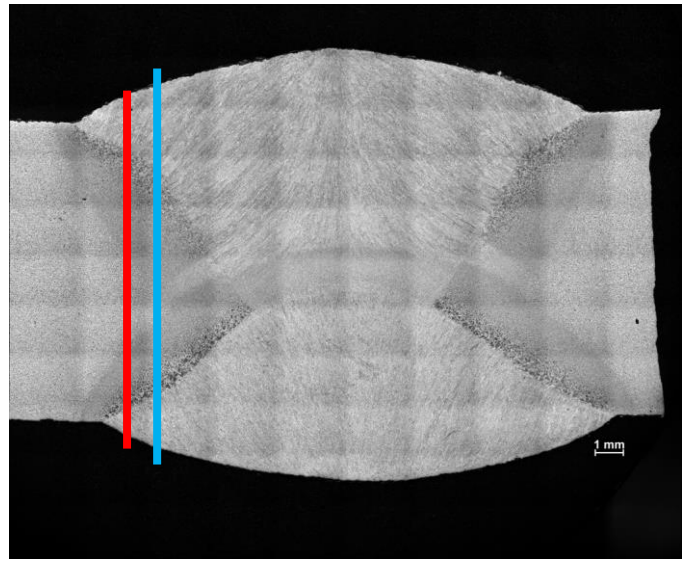

Figure 9. Image montage of the seam weld and HAZ from the vintage X52 steel, with lines showing the approximate positions where the cracks were grown (growth direction is into the image) for the two specimens tested.

which is rich in martensite. Post-test analysis will be made in the future to determine the ratios of HAZ to weld microstructures in the crack path and to quantify the amounts of key microstructures.

CONCLUSIONS

In this work, we measured FCGRs of the HAZs of three welds, two girth and one seam, from two X52 pipeline materials. Comparisons were made with corresponding base metals. The sensitivity of both the girth weld and its corresponding HAZ to hydrogen gas pressure for the vintage material is similar to that of the X52 vintage base metal. FCGR data for the HAZ of the girth weld of the modern X52 steel could only be obtained at high values of ΔK where the FCGR data for the base metal at both hydrogen gas pressures converges to the same values. Therefore, no conclusion can be made at this time regarding the sensitivity of the girth weld HAZ to hydrogen gas pressure.

The variation of the FCGR data shown by the two specimens from the HAZ of the seam weld from the vintage pipe, combined with the variation of microstructure seen in that HAZ, points toward the need for more testing of that type of HAZ. Specimens with cracks beginning at different distances from the weld should be tested so that variations in residual stress and microstructure can be evaluated. This type of systematic approach may also be necessary for the girth welds, because the most likely region of hydrogen environment-assisted corrosion may be adjacent to the fusion lines of the weld root and cap, where enlarged martensite grains are formed.

Copyright © 2015 by ASME

ACKNOWLEDGMENTS

Partial funding from this work was provided by the U.S. Department of Transportation on DTPH56-13-X-000019.

REFERENCES

1. Cialone, H., J., Holbrook, J., H., *Sensitivity of steels to degradation in gaseous hydrogen*. 962 ed. ASTM STP 962. Vol. STP. 1988: ASTM STP 962. Hydrogen Embrittlement: Prevention and Control.
2. Nanninga, N., Slifka, A., Levy, Y., White, C., *A review of fatigue crack growth for pipeline steels exposed to hydrogen*. Journal of Research of the National Institute of Standards and Technology, 2010. **115**(6): p. 437-452.
3. San Marchi, C., Stalheim, D., G., Somerday, B., P., Boggess, T., Nibur, K., A., Jansto, S., *Fracture and Fatigue of Commercial Grade API Pipeline Steels in Gaseous Hydrogen*, in *ASME Pressure Vessels & Piping Division/ K-PVP 2010 Conference*. 2010, ASME: Bellevue, Washington, USA. p. 10.
4. San Marchi, C., and Somerday, B.P. *Technical reference on hydrogen compatibility of materials: Plain carbon ferritic steels: C-Mn alloys (code 1100)*. 2010 October 2010 [cited 2012 January 3, 2012]; Available from: http://www.sandia.gov/matlsTechRef/.
5. Bolzoni, F., Cabrini, M., and Spinelli, C. *Hydrogen diffusion and hydrogen embrittlement behaviour of two high strength pipeline steels*. in *EUROCORR 2001: The European Corrosion Congress*. 2001. Lake Garda, Italy.
6. Capelle, J., Gilgert, J., Dmytrakh, I., Pluvinage, G., *Sensitivity of pipelines with steel API X52 to hydrogen embrittlement.* International Journal of Hydrogen Energy, 2008. **33**(24): p. 7630-7641.
7. Brass, A., and Chene J *Influence of tensile straining on the permeation of hydrogen in low alloy Cr-Mo steels.* Corrosion Science, 2006. **48**: p. 481-497.
8. de Santa Maria, M., and Procter, RPM *Environmental cracking (corrosion fatigue and hydrogen embrittlment) X-70 linepipe steel*. in *International Conference on Fatigue and Crack Growth in Offshore Structures*. 1986. London, England.
9. Hardie, D., Charles, EA, and Lopez, AH *Hydrogen embrittlement of high strength pipeline steels.* Corrosion Science, 2006. **48**: p. 4378-4385.
10. Duncan, A. *Tensile Testing of Carbon Steel in High Pressure Hydrogen*. in *Proceedings of the 2007 ASME Pressure Vessels and Piping/CREEPS Conference*. 2007. San Antonio, Texas, USA.
11. Nibur, K., Somerday, BP, Balch, DK, San Marchi, C, *Sustained load cracking of steels for hydrogen storage and delivery.* Effects of Hydrogen on Materials, 2008: p. 341-348.
12. Moro, I., Briottet, L, Lemione, P, Andrieu, E, Blanc, C, Odemer, G, Chene, J, Jambon, F, *Damage under high pressure hydrogen environment of a high strength pipeline steel X80.* Effects of Hydrogen on Materials, 2008.
13. Xu, K., and Rana, M, *Tensile and fracture properties of carbon and low alloy steels in high pressure hydr.* Effects of Hydrogen on Materials, 2008.
14. Suresh, S., Ritchie, R. O., *Mechanistic dissimilarities between environmentally influenced fatigue-crack propagation at near-threshold and higher growth rates in lower strength steels.* Metal Science, 1982. **16**(11): p. 529-538.
15. San Marchi, C., Stalheim, D., G., Somerday, B., P., Boggess, T., Nibur, K., A., Jansto, S., *Fracture Resistance and Fatigue Crack Growth of X80 Pipeline Steel in Gaseous Hydrogen*, in *ASME Pressure Vessels & Piping Division/ K-PVP 2011 Conference*. 2011, ASME: Baltimore, Maryland, USA. p. 9.
16. Nibur, K., San Marchi, C, and Somerday, BP. *Fracture and fatigue tolerant steel pressure vessels for gaseous hydrogen*. in *ASME 2010 Pressure Vessels & Piping Conference, PVP2010-25827*. 2010. Bellevue, WA.
17. Cialone, H., Holbrook, J., *Effects of gaseous hydrogen on fatigue crack growth in pipeline steel.* Metallurgical and Materials Transactions A, 1985. **16**(1): p. 115-122.
18. Holbrook, J.H., *Hydrogen Degredation of Pipeline Steels*. 1986, Battelle Columbus Laboratories: Brookhaven National Laboratory. p. 172.
19. Lam, P.S., Sindelar, R. L., Adams, T. M. *Literature Survey of Gaseous Hydrogen Effects on the Mechanical Properties of carbon and Low carbon Steels*. in *ASME Pressure Vessels and Piping Division Conference*. July 22-26, 2007. San Antonio, TX.
20. Amaro, R.L., Findley, K. O., Rustagi, N., Drexler, E. S., Slifka, A. J., *Fatigue Crack growth of X100 Pipeline Steels in Gaseous Hydrogen.* International Journal of Fatigue, 2014. **59**: p. 262-271.
21. Drexler, E.S., Slifka, A. J., Amaro, R. L., Barbaosa, N., Lauria, D. S., Hayden, L. E., Stalheim, D. G., *Fatigue Crack Growth Rates of API X70 Pipeline Steel in a Pressurized Hydrogen Gas Environment.* Fracture and Fatigue of Engineering Materials and Structures, 2013. **37**(5): p. 517-525.
22. Slifka, A.J., Drexler, E.S., Stalheim, D.G., Amaro, R.L., Lauria, D.S., Stevenson, A.E., and Hayden, L.E. *The effect of microstructure on the hydrogen-assisted fatigue of pipeline steels, PVP2013-97217*. in *ASME Pressure Vessel and Piping Division Conference*. 2013. Paris, France, July 14-18, 2013.
23. Slifka, A., Drexler, ES, Amaro, RL, Lauria, DS, Hayden, LE, Stalheim, DG, Chen, Y. *Summary of an ASME/DOT project on measurements of fatigue crack growth rate of pipeline steels - PVP2014-2893*. in *ASME 2014 Pressure Vessels & Piping Conference*. 2014. Anaheim, CA: ASME.
24. Moro, I., Briottet, L, Lemoine, P, Doyen, O, De Dinechin, G. *Fatigue crack growth of a C-MN steel and*

Copyright © 2015 by ASME

associated weld under hydrogen pressure. in *2012 International Hydrogen Conference*. 2012. Moran, WY: ASME Press.

25. Ronevich, J., and Somerday, BP. *Measurement of fatigue crack growth relationships for steel pipeline welds in high-pressure hydrogen gas*. in *Steely Hydrogen*. 2014. Ghent, Belgium.
26. *ASTM Standard E8/E8M-09 "Standard Test Method for Tension testing of Metallic Materials"*. 2009: West Conshohocken, PA.
27. *ASTM Standard E 647-11 "Test Method for Measurement of Fatigue Crack Growth Rates"*. 2011, ASTM International. p. 46.
28. *ASTM Standard G142-98 "Standard test method for determination of susceptibility of metals to embrittlement in hydrogen containing environments at high pressure, high temperature, or both"*. 2004, ASTM International: West Conshohocken, PA. p. 4.
29. Drexler, E.S., McColskey, J. D., Dvorak, M., Rustagi, N., Lauria, D. S., and Slifka, A. J. , *Apparatus for simultaneous fatigue testing of multiple compact tension specimens in air and controlled (harsh) environments.* Experimental Techniques, 2014: p. accepted.
30. Chen, Y., Liu, M, Wang, Y-Y, Slifka, AJ, Drexler, ES, Amaro, RL, McColskey, JD, and Hayden, LE, *Performance evaluation of high-strength steel pipelines for high-pressure gaseous hydrogen transportation*. 2013: US Dept. of Transportation-PHMSA, DOT Project DTHP56-07-0001. p. 104.

Copyright © 2015 by ASME